RSC Advances

COMMUNICATION

View Article Online
View Journal | View Issue

Cite this: *RSC Adv.*, 2016, **6**, 47907

Received 1st December 2015
Accepted 6th May 2016

DOI: 10.1039/c5ra25571f

www.rsc.org/advances

Toward rational design of palladium nanoparticles with plasmonically enhanced catalytic performance†

Anna Klinkova,*[a] Aftab Ahmed,[b] Rachelle M. Choueiri,[a] Jeffery R. Guest[b] and Eugenia Kumacheva*[a]

Palladium is a plasmonic metal, however plasmonically mediated enhancement of catalytic performance of Pd nanoparticles is underexplored. We report plasmonically mediated enhancement of catalytic performance of Pd-based nanoparticles with different shapes and internal structure. We found that Pd-only nanoparticles with geometry promoting plasmonic light concentration show stronger effect on light-induced catalytic performance than hybrid Pd-based nanoparticles with a 'canonic' plasmonic metal (Au) core. Our findings pave the way for the design, synthesis and fabrication of Pd nanocatalysts with enhanced performance under visible light illumination.

Plasmonic nanoparticles (NPs) have attracted great interest as a new class of photocatalysts utilizing solar energy.[1] The excitation of localized surface plasmon resonance (LSPR) of the NPs generates at their surface a high concentration of electrons with energy above the Fermi level (hot electrons), which can excite electronic or vibronic transitions in reagent molecules adsorbed on the NP.[2] Alternatively, hot electrons can relax *via* electron–phonon coupling with heat transfer in the surrounding medium.[3] Both of these light-mediated processes enhance catalytic performance of plasmonic NPs.[1b,4]

Photocatalytic activity of plasmonic NPs has been used in a number of chemical reactions,[1b,5] which showed a linear dependence of reaction rate on the illumination intensity and a significant difference between the rates of the reaction conducted under illumination and upon heating in dark.[4,6]

Plasmonically mediated catalysis has been generally limited to the use of Au or Ag NPs, which catalyze a limited number of reactions, compared to NPs of other transition metals.[7] In particular, Pd is a catalytically active material used in conventional catalysis of a great number of reactions. To achieve plasmonically mediated enhancement of the catalytic performance of Pd-based NPs, Pd is generally combined with a canonic Au component.[5a,5b,8] In such NPs, the Au constituent plays the role of a light harvesting antenna, while Pd acts as a catalytic component. Other combinations of Pd NPs, *e.g.*, with semiconductor light sensitising components such as CdS or CdSe have been extensively studied.[9] Yet, Pd is a plasmonic material, and the catalytic activity under plasmonic excitation of solely Pd NPs can be enhanced, if their structure is rationalized.

The effect of visible light illumination of sub-10 nm Pd NPs has been studied,[10] however, in this system, light-enhanced catalytic performance stemmed primarily from the excitation of d-band electrons. Since the LSPR of these Pd NPs is in the ultra-violet region, it may only weakly affect their catalytic activity under visible light illumination.[3] Non-spherical Pd NPs with dimensions ≥50 nm,[11] and Pd nanospheres with a diameter >70 nm (ref. 12) exhibit LSPR in the visible spectral range, however, their photocatalytic activity has not been explored.

In particular, Pd nanocubes (NCs) constitute a promising class of NPs, in which the electron confinement effect and an inhomogeneous electric field are more efficient in photogeneration of hot electrons than in spherical NPs.[13] The confinement effect is further enhanced in NCs with sharp geometric features.[14] Thus, a study of photocatalytic properties of Pd NCs with LSPR in the visible spectral range and comparing them with Au–Pd NCs is important for the design of Pd-based plasmonic nanocatalysts for reactions mediated by solar energy.

In the present work, to address the role of internal structure of Pd-based NCs, we compared the photocatalytic behavior of Pd nanocubes (NCs) and Au/Pd core–shell NCs (CS-NCs). The role of structural characteristics of Pd NPs was explored by comparing the performance of Pd NCs and Pd nanocubes with protruded edges (PE-NCs). Upon excitation at the corresponding LSPR wavelengths, the highest catalytic activity of the NPs in the reduction of 4-nitrophenol was achieved for PE-NCs, signifying the greater importance of the NP geometry than their

[a]*Department of Chemistry, University of Toronto, Toronto, Ontario M5S 3H6, Canada. E-mail: aklinkov@chem.utoronto.ca; ekumache@chem.utoronto.ca*

[b]*Center for Nanoscale Materials, Argonne National Laboratory, Argonne, Illinois 60439, USA*

† Electronic supplementary information (ESI) available: Details of the synthesis of NCs, PE-NCs, CS-NCs, catalytic experiments, electromagnetic simulations, and additional data including current density profiles and photothermal heating consideration. See DOI: 10.1039/c5ra25571f

internal structure. This trend correlated with the results of simulations of absorption, electric field enhancement and current density distribution at the NP surface. The results of this work are important in the design of Pd-based nanocatalysts acting under visible light illumination.

Fig. 1a–c shows the schematics and the scanning electron microscopy (SEM) images of Pd-based NPs used in the present work. NCs with an edge length of 50 ± 4 nm were synthesized by seed-mediated growth.[11a] The synthesis of PE-NCs with a side length of 50 ± 3 nm and protrusion height of 4 ± 2 nm was conducted using the Cu(II)-assisted seed-mediated growth.[11b] The synthesis of CS-NCs with a side length of 51 ± 3 nm included the growth of 45 ± 1 nm-size Au NCs and the synthesis of the Pd shell on the surface of Au NCs. The internal structure of CS-NCs with an Au cubic core and a 3 nm-thick Pd shell was verified using energy dispersive X-ray (EDX) mapping (Fig. 1c, inset, and Fig. S2, ESI†). We note that all NPs, including CS-NCs, were synthesized in the presence of Br^-, which is known to stabilize specifically {100} crystallographic planes of Pd.[11d] The utilization of three types of Pd-based NCs with similar dimensions, all stabilized with cetyltrimethylammonium bromide, enabled comparison of the effect of NP shape and internal structure on their photocatalytic properties.

Fig. 1d–f shows extinction spectra of the NCs, PE-NCs, and CS-NCs, all with LSPR peaks in the visible range. The spectrum of the NCs (Fig. 1f) exhibited an LSPR peak centred at 400 nm. The LSPR peak of PE-NCs at 450 nm (Fig. 1e) showed a weak red shift, compared to that of NCs, possibly, due to the increased optical polarizability of electrons at sharp PE-NC edges.[15] The spectrum of CS-NCs exhibited two distinct peaks, originating from absorption of light by the Au core and the Pd shell (Fig. 1f). Peak broadening for the CS-NCs, in comparison with the Au core, resulted from the contribution of the imaginary part of the dielectric function of Pd, which was larger than that of Au.[16]

Photocatalytic properties of the NCs, PE-NCs and CS-NCs were examined for Pd-catalyzed reduction of 4-nitrophenol (4NP) into 4-aminophenol (4AP) (see inset in Fig. 2a). Monitoring of the conversion 4NP → 4AP by UV-visible spectroscopy enables the evaluation of the catalytic properties of metal NPs.[17]

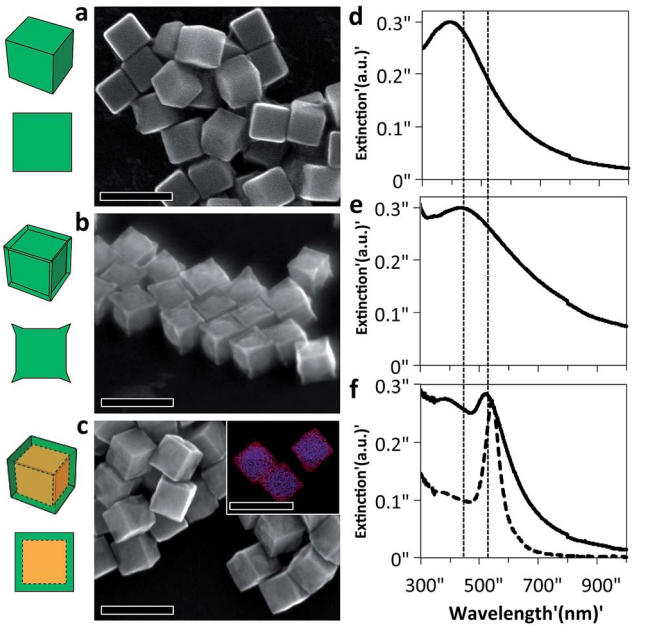

Fig. 1 Schematic illustration of 3D and 2D cross-section (left) and corresponding SEM images (right) of (a) NCs, (b) PE-NCs, and (c) CS-NCs. Green and orange colors show the Pd and Au components of the NPs, respectively. Inset in (c) shows an EDX mapping image of the core–shell Au/Pd NCs. Scale bars are 100 nm. Extinction spectra (solid lines) of aqueous solutions of (d) the NCs, (e) PE-NCs, and (f) CS-NCs. The dashed spectrum in (c) shows the spectrum of Au NC cores used for CS-NCs synthesis. Dashed lines in (d–f) show 450 and 532 nm wavelength for clarity.

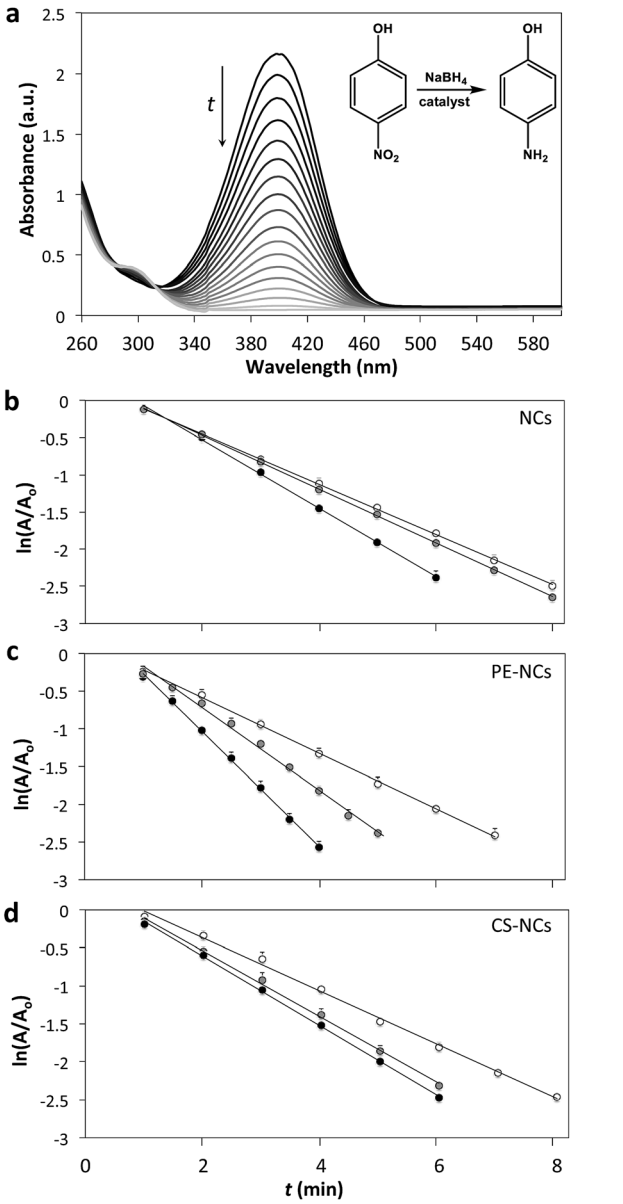

Fig. 2 (a) Evolution of the absorption spectra in the course of 4NP reduction. Inset: reaction of the reduction of 4NP. (b–d) The dependence $\ln(A/A_o)$ *vs.* *t* for 4NP reduction in dark (open symbols), under illumination at 450 nm (black symbols) and 532 nm (grey symbols) using NCs (b), PE-NCs (c), and CS-NCs (d).

In the present work, the reaction was carried out in dark and under illumination in thermostated reactor using 0.7 W laser excitation at the wavelengths of 450 and 532 nm, corresponding to the extinction maxima of PE-NCs and CS-NCs, respectively. At 450 nm the extinction of the NCs was 92% of the LSPR peak value.

In the course of the reaction, the intensity of 4NP absorption peak at 400 nm reduced, until almost complete disappearance after 8 min (Fig. 2a), indicating its close-to-complete consumption. Concurrently, a new peak developed at 300 nm, consistent with the formation of 4AP. Similar evolution of absorption spectra was observed in the presence of PE-NCs and CS-NCs (see ESI†).

Since $NaBH_4$ was added in large excess with respect to 4NP concentration, the reaction can be treated as a pseudo first-order process. The reaction rate was characterized by plotting $\ln(A/A_o)$ *vs.* the reaction time t, where A and A_o are the absorption intensity at 400 nm at time t and $t = 0$, respectively.

Fig. 2b–d shows the variation of $\ln(A/A_o)$ *vs.* t for the reaction under illumination and in dark, carried out in the presence of NCs, PE-NCs, and CS-NCs. The linear fit of these data provided the reaction rate constants determined from the slopes of the graphs. The reaction rate enhancement was defined as δ_{450} or δ_{532}, where $\delta = (k_L - k_D)/k_D$, k_L and k_D are rate constants of the reaction conducted under illumination wavelength close to LSPR of CS-NCs, the reaction rate increase was lower than that observed for pure Pd NCs at their LSPR. Although the Au core of core–shell NPs is typically considered to be a plasmonic antenna,[5a] our results show that the core–shell NP configuration had inferior performance, compared to pure Pd NCs.

Importantly, 450 and 532 nm laser beams illuminated only 7 and 3% of the solution volume, respectively (see ESI†). Thus the measured photocatalytic rate and in dark, respectively, and the subscripts 450 and 532 correspond to the illumination wavelengths.

Table 1 summarizes the results of experiments. Rate constants for the reaction conducted in the dark in the presence of NCs, PE-NCs, and CS-NCs had comparable values of 0.34, 0.37 and 0.35 min^{-1}, respectively. For the reaction under illumination, the trends shown in Table 1 can be summarized as follows. For all NP types, reaction rate increased upon LSPR excitation. A stronger rate enhancement was measured at 450 than at 532 nm. Under illumination at either 450, or 532 nm the strongest rate enhancement was observed for PE-NCs.

Based on earlier studies on plasmonically enhanced catalysis, light-mediated increase in reaction rate can result from either transient transfer of hot electrons to adsorbed molecules and/or local photothermal heating.[2–4] Direct hot electron injection into the adsorbate acceptor states plays a major role in photocatalysis by plasmonic NPs,[1a] while the heating mechanism has a minor effect at illumination intensities on the order of 100 mW cm^{-2}.[1a,4] We performed control experiments in dark at different temperatures to evaluate the contribution of the photothermal effect, and demonstrated that at light intensities used in the current work ($\sim 10^4$ mW cm^{-2}) it should not be primarily responsible for the observed rate enhancements (see ESI† for details). Thus, at light intensities used in the present work, both photothermal heating and hot electron injection mechanisms may contribute to reaction rate enhancement.

We emphasize that elucidating the relative contributions of the two mechanisms is beyond the scope of this work, however, both of them are influenced by electric field (E-field) enhancement and current density (J) in the NPs. Plasmon-induced electromagnetic field contributes to a stronger interaction between NPs and molecular adsorbates and can induce transitions of electrons from occupied to unoccupied states.[2] In addition, the energy gained by electrons upon plasmonic excitation (characterized by current density) can dissipate into heat. Based on Ohm's law, heat dissipated per unit volume is given by the product of local E-field and J, leading to local temperature increase.[18]

To gain insight into the role of shape and composition of NCs, PE-NCs, and CS-NCs on their plasmonic properties and photocatalytic performance, we performed Finite-Difference Time-Domain (FDTD) simulations. The NPs were modelled using a fit to the experimental data of Johnson and Christy (for Au) and Palik (for Pd).[19] Scattering, absorption and extinction cross-sections were calculated using the formalism of total field scattered field.[20]

Fig. 3a–c shows the variation in extinction, scattering, and absorption properties of the NPs. The simulated spectra were in agreement with experimental results shown in Fig. 1d–f. Fig. 3d–i shows E-field enhancement at the NP corners as a function of the excitation wavelength. The E-field was mostly concentrated at the sharp features of the NPs (Fig. 3d–f). The current density was also concentrated at NP edges and corners (see ESI†). The use of NPs with sharp features led to strong E-field enhancement and high J, while the introduction of Au in the interior of Pd NC mainly resulted in the shift of E-field and J maxima toward longer wavelengths.

Fig. 3 shows the correlation of the maximum in E-field enhancement with the LSPR peaks for the NCs, PE-NCs, and CS-NCs (the value of J exhibited a similar trend). Notably, the PE-NCs exhibited the strongest E-field and J, which correlated

Table 1 Rate constants of 4NP reduction using Pd NCs, PE-NCs, and CS-NCs in the dark and under laser illumination

	LSPR[a] [nm]	k_D [min^{-1}]	k_L at 450 nm illumination [min^{-1}]	δ_{450}	k_L at 532 nm illumination [min^{-1}]	δ_{532}
NCs	400	0.34	0.46	36%	0.36	7%
PE-NCs	450	0.37	0.76	107%	0.55	46%
CS-NCs	395, 532	0.35	0.46	31%	0.44	23%

[a] LSPR correspond to those shown in Fig. 1d–f.

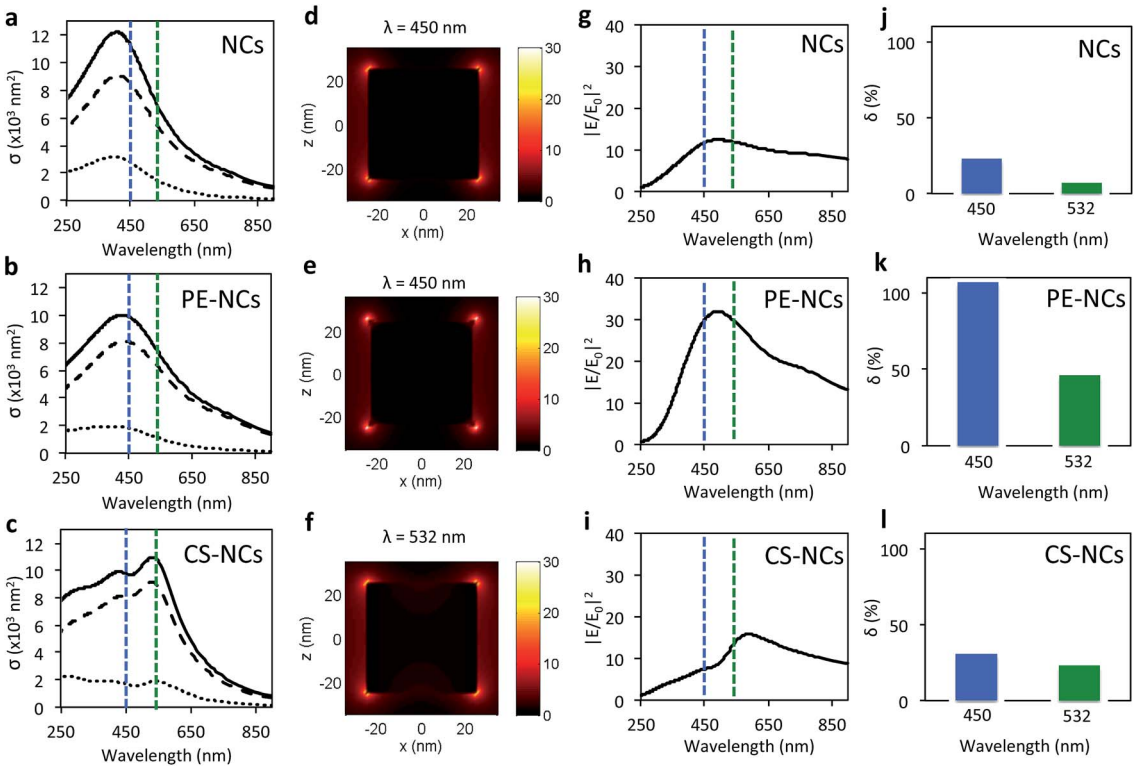

Fig. 3 FDTD simulations of (a–c) extinction (solid lines), scattering (dotted lines), and absorption spectra (dashed lines) of NCs (a), PE-NCs (b), and CS-NCs (c). (d–f) E-field enhancement profiles (log-scale) of the 2D cross-section at $y = 0$ nm of NCs (d), PE-NCs (e), and CS-NCs (f). The incident plane wave is x-polarized. (g–i) E-field intensity at the cube corners for NCs (g), PE-NCs (h), and CS-NCs (i). Rate enhancements compared to reactions in dark, δ_{450} (blue) and δ_{532} (green), observed in the experimental catalytic reduction of 4NP using NCs (j), PE-NCs (k), and CS-NCs (l) under laser illumination are shown for comparison.

with the highest measured reaction rate increase. In addition, for the NCs and PE-NCs, the value of J at 450 nm excitation was higher than at 532 nm.

A stronger than expected enhancement in the reaction rate at 450 nm excitation, compared to 532 nm, was observed for all NP types. This trend may be due to the contribution of direct excitation of 4NP at this wavelength (Fig. 2a), or the contribution of the d-band electron excitation in Pd, generating additional hot electrons.[10] Second, since the apparent reaction rates characterize the average reaction rate for the entire NP surface, the actual local increase in reaction rate at sharp NP features can be significantly higher.

Conclusions

In conclusion, the introduction of sharp geometric features in Pd PE-NCs leads to a higher efficiency of these NPs in plasmonically mediated catalysis, in comparison with Pd NCs and CS-NCs. This effect signifies a dominant effect of NP shape in their plasmonically enhanced catalytic performance. Introduction of Au component, a 'canonic' plasmonic metal inside Pd NCs can enhance the photocatalytic performance of the composite NPs under illumination at longer wavelengths, as it red-shifts their extinction maximum, in comparison with Pd-only NCs. Given that NPs with sharp geometric features enclosed by high index facets are often more efficient in catalytic reactions,[21] than NPs with low index facets, plasmonic photocatalysis on NPs with a maximized number of sharp features offers a route to enhancing their catalytic performance. Further exploration of plasmonic properties of Pd NPs and other non-canonic plasmonic transition metal NPs with sharp geometrical features would open up new avenues for applications of plasmon-induced photocatalysis.

Acknowledgements

A. K. thanks I. Gourevich and N. Coombs for help with SEM imaging and EDX. A. K., R. M. C. and E. K. thank Connaught fund for financial support of this work. A. K. acknowledges Ontario Trillium Scholarship, R. M. C. acknowledges Natural Sciences and Engineering Research Council of Canada for a PGS-D scholarship. J. R. G. thanks Yugang Sun for helpful discussions. Use of the Center for Nanoscale Materials, an Office of Science user facility, was supported by the U. S. Department of Energy, Office of Science, Office of Basic Energy Sciences, under Contract No. DE-AC02-06CH11357.

Notes and references

1 (*a*) M. J. Kale, T. Avanesian and P. Christopher, *ACS Catal.*, 2014, **4**, 116; (*b*) X. Lang, X. Chen and J. Zhao, *Chem. Soc. Rev.*, 2014, **43**, 473.

2 M. L. Brongersma, N. J. Halas and P. Nordlander, *Nat. Nanotechnol.*, 2015, **10**, 25.
3 J. G. Smith, J. A. Faucheaux and P. K. Jain, *Nano Today*, 2015, **10**, 67.
4 P. Christopher, H. Xin and S. Linic, *Nat. Chem.*, 2011, **3**, 467.
5 (*a*) F. Wang, C. Li, H. Chen, R. Jiang, L.-D. Sun, Q. Li, J. Wang, J. C. Yu and C.-H. Yan, *J. Am. Chem. Soc.*, 2013, **135**, 5588; (*b*) X. Huang, Y. Li, Y. Chen, H. Zhou, X. Duan and Y. Huang, *Angew. Chem., Int. Ed.*, 2013, **52**, 6063; (*c*) M. A. Mahmoud, B. Garlyyev and M. A. El-Sayed, *J. Phys. Chem. Lett.*, 2015, **5**, 4088; (*d*) J. Lee, S. Mubeen, X. Ji, G. D. Stucky and M. Moskovits, *Nano Lett.*, 2012, **12**, 5014.
6 S. Mukherjee, F. Libisch, N. Large, O. Neumann, L. V. Brown, J. Cheng, J. B. Lassiter, E. A. Carter, P. Nordlander and N. J. Halas, *Nano Lett.*, 2013, **13**, 240.
7 D. Astruc, *Nanoparticles and Catalysis*, Wiley-VCH, Weinheim, 2008.
8 S. Sarina, H. Zhu, E. Jaatinen, Q. Xiao, H. Liu, J. Jia, C. Chen and J. Zhao, *J. Am. Chem. Soc.*, 2013, **135**, 5793.
9 U. Banin, Y. Ben-Shahar and K. Vinokurov, *Chem. Mater.*, 2014, **26**, 97.
10 S. Sarina, H.-Y. Zhu, Q. Xiao, E. Jaatinen, J. Jia, Y. Huang, Z. Zheng and H. Wu, *Angew. Chem., Int. Ed.*, 2014, **53**, 2935.
11 (*a*) W. Niu, L. Zhang and G. Xu, *ACS Nano*, 2010, **4**, 1987; (*b*) W. Niu, W. Zhang, S. Firdoz and X. Lu, *Chem. Mater.*, 2014, **26**, 2180; (*c*) Y. Xiong, J. Chen, B. Wiley, Y. Xia, Y. Yin and Z.-Y. Li, *Nano Lett.*, 2005, **5**, 1237; (*d*) S.-H. Yoo, J.-H. Lee, B. Delley and A. Soon, *Phys. Chem. Chem. Phys.*, 2014, **16**, 18570.
12 K. Sugawa, H. Tahara, A. Yamashita, J. Otsuki, T. Sagara, T. Harumoto and S. Yanagida, *ACS Nano*, 2015, **9**, 1895.
13 H. Zhang and A. O. Govorov, *J. Phys. Chem. C*, 2014, **118**, 7606.
14 B. Sharma, R. R. Frontiera, A.-I. Henry, E. Ringe and R. P. Van Duyne, *Mater. Today*, 2012, **15**, 16.
15 X. Lu, M. Rycenga, S. E. Skrabalak, B. Wiley and Y. Xia, *Annu. Rev. Phys. Chem.*, 2009, **60**, 167.
16 F. Hao and P. Nordlander, *Chem. Phys. Lett.*, 2007, **446**, 115.
17 (*a*) M. A. Mahmoud and M. A. El-sayed, *ChemCatChem*, 2014, **6**, 3540; (*b*) Z. Jin, F. Wang, J. Wang, J. C. Yu and J. Wang, *Adv. Funct. Mater.*, 2013, **23**, 2137.
18 A. O. Govorov and H. H. Richardson, *Nano Today*, 2007, **2**, 30.
19 (*a*) P. B. Johnson and R. W. Christy, *Phys. Rev. B: Solid State*, 1972, **6**, 4370; (*b*) E. D. Palik, *Handbook of optical constants of solids*, Academic Press, 1998, vol. 3.
20 A. Lee, G. F. S. Andrade, A. Ahmed, M. L. Souza, N. Coombs, E. Tumarkin, K. Liu, R. Gordon, A. G. Brollo and E. Kumacheva, *J. Am. Chem. Soc.*, 2011, **133**, 756.
21 (*a*) W. Ludwig, A. Savara, R. J. Madix, S. Schauermann and H.-J. Freund, *J. Phys. Chem. C*, 2012, **116**, 3539; (*b*) M. Crespo-Quesada, A. Yarulin, M. Jin, Y. Xia and L. Kiwi-Minsker, *J. Am. Chem. Soc.*, 2011, **133**, 12787.